

Meson-polariton and string dynamics via cavity coupling in Rydberg atom arrays

Zeno Bacciconi,¹ Hernan B. Xavier,^{1,2} Matteo Marinelli,³ Devendra Singh Bhakuni,² and Marcello Dalmonte²

¹*International School for Advanced Studies (SISSA), Via Bonomea 265, I-34136 Trieste, Italy*

²*The Abdus Salam International Centre for Theoretical Physics (ICTP), Strada Costiera 11, 34151 Trieste, Italy*

³*University of Trieste, Physics Department, Via A. Valerio 2, 34127 Trieste, Italy*

(Dated: January 9, 2025)

We investigate the real time meson and string dynamics of one dimensional Rydberg atom arrays in presence of a collective cavity mode. We derive an effective description in terms of a Tavis-Cummings-Ising model, whose phase diagram features ordered and disordered phases. Single domain walls on top of ordered states behave differently from those found in Ising models, featuring strong anisotropy because of the $U(1)$ invariant coupling between light and matter. The non-local nature of the cavity mode is instead affecting meson and string dynamics drastically. Meson hybridizes coherently with the cavity photons, leading to composite meson-polariton excitations. Strings, differently from local interacting theories, acquire a finite kinetic energy and propagate freely thanks to the non-local interaction between the underlying domain-walls mediated by the cavity mode. We conclude by examining the effect of cavity losses, proposing a state-preparation protocol which actively uses the cavity mode, and presenting a concrete experimental blueprint.

Introduction. - There is presently considerable interest in exploring the real time dynamics of strongly interacting quantum matter in quantum simulators and computers [1, 2]. A major goal of this endeavor is to shed light on the role of low-lying excitations, in particular, in the context of gauge theories and spin models, where basic constituents such as mesons and strings play a prominent role [3–9]. Remarkable recent experiments have begun to investigate this within the realm of Abelian gauge theories as well as Ising-like models, exploring string [10–15] as well as meson-driven dynamics [16, 17] and false-vacuum decay [18, 19]. The dynamics considered so far has been driven by local couplings, which severely constrain the effective interactions between quasiparticles. That is not generally the case for cavity embedded quantum matter [20–24], an emerging class of quantum many body systems characterized by the interplay between local degrees of freedom (atoms [25–30], spin [31–40], electrons [41–48]) and non-local cavity modes — leading to a plethora of phenomena not accessible in traditional spin models. It is thus an open question whether such couplings to global modes can give rise to qualitatively new meson and string dynamics, and whether that can be experimentally probed.

In this work, we consider a setup consisting of an array of neutral atoms, whose ground state is coupled to a Rydberg state via a two-photon transition involving a cavity field, see Fig 1(a). Our proposal builds upon and combines outstanding achievements in the field of cavity QED [25, 49, 50] and Rydberg atom experiments [11, 51, 52], with the promise of achieving unexplored regimes where both local and non-local interactions are dominating over cavity losses and realize coherent light-matter many body dynamics.

Within this setting, locally interacting spins couple to a global mode in a controllable manner, realizing a perfect setting where to investigate hybrid meson and

string dynamics. After deriving the phase diagram of the model, we show that the cavity field has a drastic impact on its low-energy dynamics: different types of solitons emerge, featuring very distinct energetics due to cavity-assisted processes. Some of the solitons can propagate freely thanks to the cavity, while others are dynamically blocked, and effectively stay confined due to energetics.

The effect of light onto composite objects is drastic. Meson quasiparticles hybridize with light, generating a meson-polariton excitation that immediately de-localizes single mesons. In deconfined regimes instead, mesons melt during the real-time dynamics via a multi-stage local process involving a combination of spin and cavity excitations. String dynamics is instead informative about the fate of confinement in the presence of light. Remarkably we observe that strings, independently of their length, always acquire a finite kinetic energy, contrasting with local spin models where this is typically exponentially suppressed. This is due to cavity-mediated long-range interactions solitons, allowing for an exchange between string tension and kinetic energy. We illustrate this new class of dynamical behavior using exact (ED) and matrix product states (MPS)[53–57] simulations, and conclude our work by detailing a realistic experimental proposal.

Model Hamiltonian. - We consider a collection of N Rydberg atoms coupled to single cavity mode via a two photon transition through a far detuned intermediate state (see Fig. 1). This can be mapped onto a Tavis-Cumming model with an antiferromagnetic Ising interaction, in abbreviation Tavis-Cumming-Ising or TC-Ising. The Hamiltonian is [58]:

$$\hat{H} = \delta \hat{a}^\dagger \hat{a} + h_z \sum_j (-1)^j \hat{\sigma}_j^z + V \sum_j \hat{\sigma}_j^z \hat{\sigma}_{j+1}^z + g \sum_j (\hat{a} \hat{\sigma}_j^+ + \hat{a}^\dagger \hat{\sigma}_j^-) + \lambda \hat{a}^\dagger \hat{a} \sum_j \hat{\sigma}_j^z, \quad (1)$$

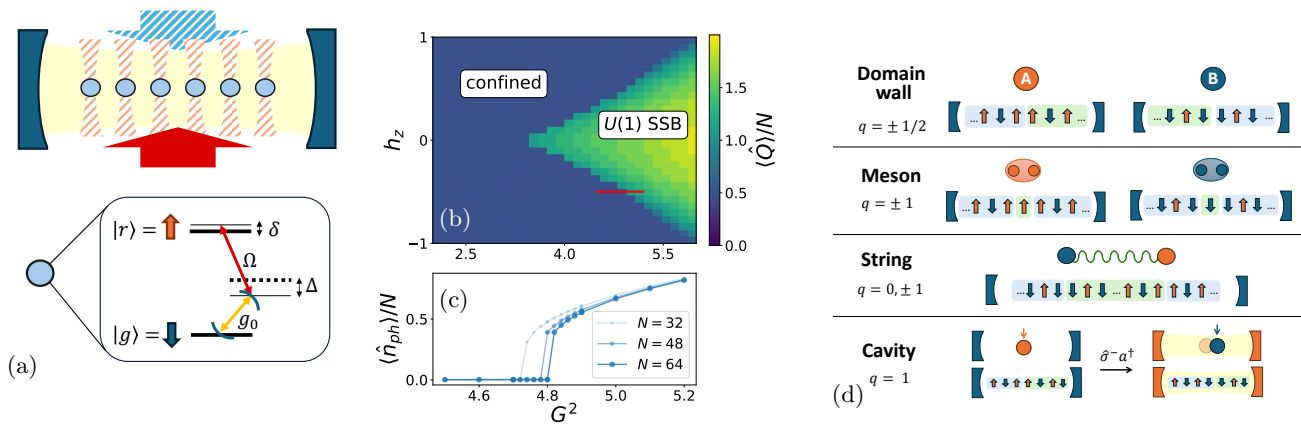


FIG. 1. (a) Sketch of the set-up under consideration, an array of individually controlled rydberg atoms coupled to a cavity mode via a two-photon transition assisted by an external laser Ω , giving a tunable coupling $g = \Omega g_0 / \Delta$. (b-c) Phase diagram of the TC-Ising model as a function of h_z and $G = g\sqrt{N}$ via (b) the ground state charge sector Q (ED and $N = 10$) and (c) photon number (DMRG); the latter at a fixed $h_z = -0.5$ and varying G (red line of (b)). (d) Sketch of the relevant low-energy degrees of freedom and their $U(1)$ charge in the confined antiferromagnetic phase.

where δ is the cavity detuning, h_z a staggered longitudinal field, V the Rydberg-Rydberg interaction truncated to the nearest neighbor, g the effective cavity-atom coupling strength and λ a cavity dependent Stark shift. We set $\lambda = 0$ for simplicity and $V = 1$.

Importantly the model has a $U(1)$ symmetry associated to the number of photons and Rydberg excitations:

$$\hat{Q} = \hat{a}^\dagger \hat{a} + \sum_j \hat{\sigma}_j^+ \hat{\sigma}_j^- . \quad (2)$$

In Fig. 1(b,c) we show the phase diagram obtained with exact diagonalization (ED) and matrix product state (MPS) simulations as a function of the *collective* light-matter interaction $G = g\sqrt{N}$ and the longitudinal staggered field h_z with fixed interaction $V = 1$. Two phases are present (see Fig. 1(c)), distinguished by the charge sector Q in which the ground state lives. The ground state is antiferromagnetic when $Q = N/2$, corresponding to the confined phase. When the charge Q instead changes we find an in-plane ferromagnet with spontaneous symmetry breaking (SSB) of the continuous $U(1)$ symmetry related to the charge Q [36, 59–61]. In Fig. 1(c) we show the photon occupation for large systems obtained with DMRG, highlighting the first order nature of the transition [58]. We further note that the phase diagram structure is quite similar to the Ising model, with the difference that the transverse field h_x is now represented by a degree of freedom in its own which, instead of driving a transition towards a *disordered* phase, drives a transition to a differently ordered state. In this sense it is also possible to understand the nature of the AFM phase as a *confined* phase of a Z_2 lattice gauge theory, as for the Ising model with a longitudinal field. Note that also Dicke-Ising models [37, 62] show a very similar phase diagram, with the important difference that the SSB is

of a discrete Z_2 instead of a continuous $U(1)$ symmetry.

In the following we will focus only on the AFM, or confined, phases dynamical properties by studying the low energy excitations depicted in Fig 1(c). Note also that as long as the cost of creating a pair of domain walls $4V$ is larger than the light-matter collective coupling $g\sqrt{N}$, their number is going to be approximately conserved.

Domain-wall propagation - The presence of a global $U(1)$ symmetry induces strong differences between domain walls formed by up-up or down-down spins, unlike the standard phenomenology of Z_2 symmetric Ising models. We thus introduce two domain wall densities:

$$\hat{D}_j^A = |\uparrow_j \uparrow_{j+1}\rangle \langle \uparrow_j \uparrow_{j+1}| \quad \hat{D}_j^B = |\downarrow_j \downarrow_{j+1}\rangle \langle \downarrow_j \downarrow_{j+1}| \quad (3)$$

which measure the presence of domain walls of type A or B at the bond between atom j and $j+1$ ($j = 0, \dots, N-1$). We study quenches of the light-matter interaction g , starting from initial classical domain wall states (Fig. 1(c)) with zero cavity photons. We remark that the system has no quantum dynamics in absence of g .

In Fig. 2 we show ED results for the propagation of type A (top row) and type B (bottom row) domain walls in two different regimes for the cavity detuning ($\delta = 1$ and $\delta = 0$). The timescale of the cavity-induced dynamics is different in all four resulting cases but can be understood by simple perturbation theory. Starting from the cavity detuned regime, $\delta = 1$, for domain walls of type A we have a second-order process:

$$|\uparrow\uparrow\uparrow\uparrow\rangle |0\rangle \rightarrow |\uparrow\uparrow\downarrow\uparrow\rangle |1\rangle \rightarrow |\uparrow\uparrow\uparrow\uparrow\rangle |0\rangle, \quad (4)$$

with a rate $J_A = g^2/\delta$. The peculiarity of this process is that the domain wall can only jump by two sites and will remain type A, as indeed clear in Fig. 2(a). Type B domain walls instead can only move through creation

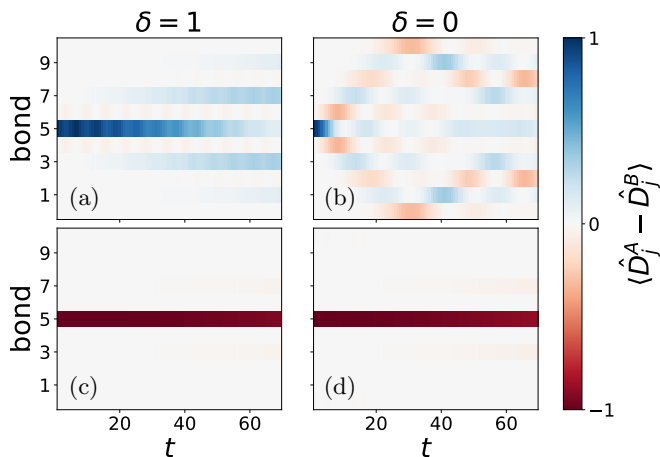


FIG. 2. Single domain wall cavity-mediated dynamics via domain wall density $\langle \hat{D}_j^A - \hat{D}_j^B \rangle$ obtained with ED. The system is initialized in a classical state with a single domain wall either of (a,b) type A or type B (c,d). The cavity photon energy is $\delta = 1$ on the left (a,c) while $\delta = 0$ on the right (b,d). $N = 12$, $g = 0.12$ and $h_z = 0$.

and destruction of other domain walls, thus costing much more energy. At lowest order:

$$|\uparrow\uparrow\downarrow\downarrow\uparrow\downarrow\rangle|0\rangle \rightarrow |\uparrow\uparrow\downarrow\downarrow\uparrow\downarrow\rangle|1\rangle \rightarrow |\uparrow\uparrow\downarrow\downarrow\uparrow\downarrow\rangle|0\rangle, \quad (5)$$

with a rate $J_B = g^2/(\delta + 4V)$ which effectively result in an apparent freezing of the domain wall.

Moving to small photon frequencies $\delta < g$ the propagation mechanism changes. The main difference is that, instead of being virtually populated by second-order processes, now the cavity can be resonantly populated. For example starting from a domain wall of type A we have:

$$|\uparrow\uparrow\uparrow\uparrow\uparrow\rangle|0\rangle \rightarrow |\uparrow\uparrow\uparrow\downarrow\uparrow\rangle|1\rangle \quad (6)$$

happening with a rate g . Here the domain wall type can oscillate between A and B during the propagation as a photon is coherently exchanged back and forth. The other case of an initial condition with a domain wall of type B (and no initial photons) does not allow these resonant processes but only the second order processes thus still giving a frozen dynamics.

Meson-polaritons - Another important low-energy excitation which can be built on top of an AFM ground state is a single spin-flip, i.e., a magnon or, in connection with the LGT interpretation, a meson. As for domain walls, we can identify two different type of mesons A and B corresponding respectively to a spin flipped up (\downarrow to \uparrow) and vice versa. In particular at $g = 0$ the simplest meson states are classical configurations:

$$|\pi_j^{A/B}\rangle|0\rangle = \hat{\sigma}_j^\pm |AFM\rangle|0\rangle \quad (\text{for } j \text{ odd/even}) \quad (7)$$

where $|AFM\rangle$ is the Néel state with up (down) spins on even (odd) sublattices and $|0\rangle$ the cavity vacuum. In

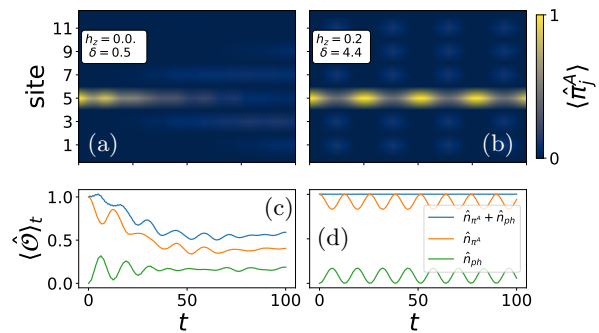


FIG. 3. Meson-polariton dynamics (a,c) in a de-confined case ($h_z = 0$, $\delta = 0.5$) and (b,d) in a confined case ($h_z = 0.2$, $\delta = 4.4$) obtained with ED. Top panels (a,b) show the dynamics in real space via the meson density, while bottom panels (c,d) show the evolution in time of key observables (total meson number, photon number and their sum). $g = 0.1$ and $N = 13$.

order to track the dynamics of these excitations we use the classical, type resolved, meson density:

$$\begin{aligned} \hat{\pi}_j^A &= |\uparrow_{j-1}\uparrow_j\uparrow_{j+1}\rangle\langle\uparrow_{j-1}\uparrow_j\uparrow_{j+1}|, \\ \hat{\pi}_j^B &= |\downarrow_{j-1}\downarrow_j\downarrow_{j+1}\rangle\langle\downarrow_{j-1}\downarrow_j\downarrow_{j+1}|. \end{aligned} \quad (8)$$

In Fig. 3 we study the meson dynamics [63] starting from a classical meson state (Eq. 7) in different regimes for h_z and δ , keeping $g = 0.1$. The leftmost panels (a,c) show the dynamics in absence of confinement $h_z = 0$. Here the two domain walls forming the meson split-up and propagate independently, as highlighted by a quickly decaying meson number $\hat{n}_{\pi^A} = \sum_j \hat{\pi}_j^A$. In the right panels (b,d), we show the emergence of confinement with a finite $h_z = 0.2$ for a cavity detuning $\delta = 4V + 2h_z = 4.4$. Note that, despite confinement, only the combined sum (blue) of number of photons (green) and meson (orange) is conserved. This hybridization can be traced back to the formation of collective meson-polariton states which imprint a non-local dynamics on the initially local meson excitation, i.e., a de-localization of the meson on the whole spin-chain. In order to better understand the physics at play, we explicitly construct the collective states responsible for the meson-polariton formation:

$$|C_1\rangle = |AFM\rangle|1\rangle, \quad |C_2\rangle = \frac{1}{\sqrt{N_{\text{odd}}}} \sum_{j \text{ odd}} |\pi_j^A\rangle|0\rangle. \quad (9)$$

The dynamics within this subspace then reduces to a simple two-level system dynamics:

$$\langle C_i | \hat{H} | C_j \rangle = \begin{pmatrix} \delta & g\sqrt{N_{\text{odd}}} \\ g\sqrt{N_{\text{odd}}} & 4V + 2h_z \end{pmatrix} + \text{const.} \quad (10)$$

Kinetic terms for the mesons are order g^4 and thus neglected in this simple picture. Still from the two state model dynamics we can readily understand three important properties. (i) The non-local meson-polariton oscillations are collective, controlled by $G = g\sqrt{N}$, while

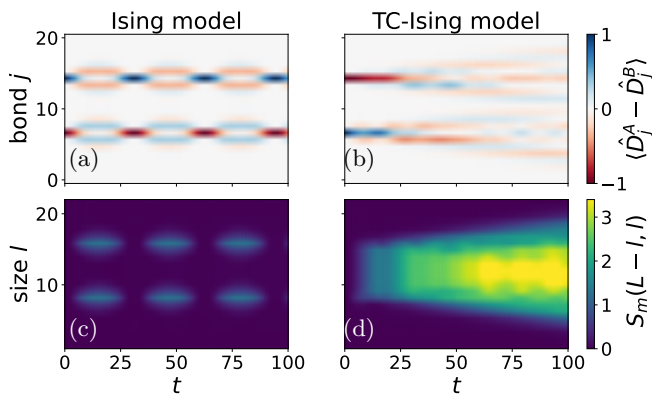


FIG. 4. String dynamics comparison between Ising model (a,c) and TC-ising model (b,d) obtained with TDVP. Top panels (a,b) show the domain wall density while the bottom panel (c,d) present the bipartite mutual information $S_m(L-l, l)$. In order to have comparable dynamics, we set $h_x = 0.1$ in the Ising case and $g = 0.1$ in the TC-Ising one with $\delta = 0.$; both cases have $h_z = 0.2$ and $N = 23$.

the local dynamics is controlled by g . (ii) At resonance, $\delta = 4V + 2h_z$ there is a stronger hybridization giving rise to coherent Rabi oscillations. (iii) A local meson has a vanishing overlap $1/\sqrt{N_{\text{odd}}}$ with the collective states, thus limiting the amplitude of the Rabi oscillations.

String dynamics - In the context of confining LGT theories, an important role is played by *string* excitations, namely bound states of two distant elementary excitations. In the simple case of the Ising model, two distant domain walls feel a confining potential proportional to their separation r_0 and the longitudinal field h_z . This induces an exponentially slow dynamics $(h_x/h_z)^{r_0}$ due to the underlying locality of the LGT dynamics (represented by a local transverse field h_x). This phenomenology is lost in the TC-Ising model where, independently of r_0 , distant domain walls can interact via the exchange of cavity photons. We illustrate this fundamental difference in Fig. 4 by direct comparison of the real-time evolution of a string in the two cases of Ising model (a,c) and TC-ising model (b,d), obtained via time-dependent variational principle (TDVP) simulations [55, 58]. The domain wall density (top panels) clearly shows that in the local Ising case strings are effectively immobile, while in the TC-Ising case strings can have a finite kinetic energy, comparable to that of single domain walls (Fig. 2). In particular the process which allow for the motion of arbitrary length strings r_0 is the following:

$$\begin{aligned}
 & \overbrace{|\dots\uparrow\uparrow\uparrow\uparrow\uparrow\uparrow\downarrow\downarrow\downarrow\dots\rangle}_{r_0} |0\rangle \rightarrow \overbrace{|\dots\downarrow\downarrow\downarrow\downarrow\downarrow\downarrow\uparrow\uparrow\uparrow\dots\rangle}_{r_0-1} |1\rangle \rightarrow \\
 & \rightarrow \overbrace{|\dots\uparrow\downarrow\downarrow\uparrow\uparrow\downarrow\uparrow\downarrow\uparrow\dots\rangle}_{r_0} |0\rangle
 \end{aligned} \quad (11)$$

with a rate $J_s = g^2/(\delta \pm 2h_z)$ depending on whether the hopping is towards the direction where the type A

domain wall is or not.

In order to confirm that the important emergent dynamical degree of freedom is the string and that single domain walls do not move independently, we calculate the mutual information (Fig 4(c,d)) between two subsystem of length l and $L-l$:

$$S_m(L-l, l) = S(\rho_{1..l}) + S(\rho_{l+1..L}) - S(\rho_c), \quad (12)$$

where $S(\rho_X)$ is the von Neumann entropy of a subsystem X being either the first l atoms, the last $L-l$ atoms or the cavity c . In the case of the Ising model this just reduces to twice the bipartite entanglement entropy. The important different feature distinguishing the Ising and TC-Ising case is the presence of a *plateau* already at early times ($t \lesssim 50$) when the bipartition length l varies along the string ($8 < l < 14$). This highlights the immediate build-up of long-range correlations between the two domain walls forming the end of the string, which then can move coherently as a single object via the exchange of virtual photons.

Experimental blueprint. - The proposed experimental implementation uses ^{87}Rb atoms trapped in optical tweezers, though the model Hamiltonian and excitation scheme described above are applicable to a range of atomic species, including alkali [64] and alkaline-earth-like atoms [65]. Rydberg control is achieved via a two-photon excitation from the ground state $|g\rangle = |5S_{1/2}, F=2, m_F=-2\rangle$ to the Rydberg state $|r\rangle = |70S_{1/2}, J=1/2, m_J=-1/2\rangle$ via an intermediate state $|e\rangle = |6P_{3/2}, F=3, m_F=-3\rangle$ [11]. This transition is driven by circularly polarized lasers at wavelengths of 420 nm and 1013 nm, respectively, with an intermediate state detuning $\Delta \simeq 2\pi \times 0.5$ GHz. The set-up allows for a simple state preparation scheme of specific initial states [58].

The one-dimensional array of atoms is coupled to a bow-tie cavity that sustains two counter-propagating unidirectional modes, of opposite circular polarization. This configuration balances the requirements of strong cavity coupling, compatibility with Rydberg physics, and scalability to large atom arrays. The cavity design provides substantial optical access, enabling hundreds of optical tweezers for single-atom control while maintaining a large distance between the atoms and the dielectric surfaces of the mirrors, thereby mitigating stray charge effects on Rydberg atoms [66]. Importantly, this design also achieves small mode volumes, ensuring the strong cavity coupling essential for the proposed implementation [67].

Assuming a cavity waist (w_0) of $3\mu\text{m}$, a cavity length of 6.9cm , a finesse of 50000 along with the measured decay rates and branching ratios of the $6P_{3/2}$ states [68], the cavity parameters are $\{g_0, \kappa, \Gamma\} = 2\pi \times \{800\text{ kHz}, 20\text{ kHz}, 1.35\text{ MHz}\}$. Here, g_0 represents the on-resonance atom-cavity coupling, κ denotes the half-linewidth of the cavity, and Γ the full linewidth of the

intermediate state. Notably, planar ring cavities with similar w_0/λ_C ratios have already been demonstrated for the same finesse [67].

In order to minimize off-resonant scattering from the intermediate state ($\Gamma\Omega^2/\Delta^2$) and maximize the two-photon transition strength ($g_0\Omega/\Delta$), we propose to operate the 1013 nm laser at a Rabi frequency $\Omega \simeq \Delta/10 \simeq 2\pi \times 50$ MHz. This, using the dimensionless coupling $g/V = g_0\Omega/\Delta = 0.1$ used in most of the results, leads to realistic rates for atom loss $\gamma_{at}/V \simeq 0.016$ and photon loss $\kappa/V \simeq 0.025$ which justify the timescales $t \lesssim 100$ up to which all results are presented. We also remark that, for the dynamics studied in this work, the effect of photon loss is not severe due to the small population of the cavity mode [58].

Conclusions - We have studied real-time dynamics of low energy excitations in a Tavis-Cummings-Ising model. This highlights the non-trivial interplay between local and non-local degree of freedoms, contrasted with usual locally interacting models. Real time and space resolved dynamics in particular is key to distinguish the degree of “locality” of the emergent composite excitations in the confined phase. We further expect new interesting physics arising also in the deconfined phase, where non-local interactions dominate from the start giving rise to an otherwise forbidden continuous $U(1)$ SSB in one dimension [36]. All these phenomena naturally arise in a simple combination of two well-developed quantum simulation platforms, Rydberg atom arrays [11, 51] and atomic cavity QED [25, 49]. Nonetheless, the physical ideas explored in such simple setting can be translated to other cavity embedded quantum many-body systems [21–24], where local and non-local emergent quasi-particles coexist.

Acknowledgments - We thank T. Chanda, D. Chang, M. Collura, M. Oehlgren and F. Scazza for discussions. MPS based simulations have been carried out with the help of the libraries ITensors.jl [69] and TenNetLib.jl [70]. ED and quantum trajectory base simulations have been carried out with QuTip [71]. M.D. was partly supported by the QUANTERA DYNAMITE PCI2022-132919. M.D. was supported by the EU-Flagship programme Pasquans2, by the PNRR MUR project PE0000023-NQSTI, the PRIN programme (project Co-QuS), and the ERC Consolidator grant WaveNets. H. B. X. was supported by the MIUR programme FARE (MEPH).

[1] I. Buluta and F. Nori, Quantum simulators, *Science* **326**, 108–111 (2009).
 [2] J. I. Cirac and P. Zoller, Goals and opportunities in quantum simulation, *Nature Physics* **8**, 264–266 (2012).
 [3] E. Zohar, J. I. Cirac, and B. Reznik, Quantum simulations of lattice gauge theories using ultracold atoms in op-

tical lattices, *Reports on Progress in Physics* **79**, 014401 (2015).
 [4] M. Dalmonte and S. Montangero, Lattice gauge theory simulations in the quantum information era, *Contemporary Physics* **57**, 388–412 (2016).
 [5] M. C. Bañuls, R. Blatt, J. Catani, A. Celi, J. I. Cirac, M. Dalmonte, L. Fallani, K. Jansen, M. Lewenstein, S. Montangero, C. A. Muschik, B. Reznik, E. Rico, L. Tagliacozzo, K. Van Acoleyen, F. Verstraete, U.-J. Wiese, M. Wingate, J. Zakrzewski, and P. Zoller, Simulating lattice gauge theories within quantum technologies, *The European Physical Journal D* **74**, 10.1140/epjd/e2020-100571-8 (2020).
 [6] C. W. Bauer, Z. Davoudi, A. B. Balantekin, T. Bhattacharya, M. Carena, W. A. de Jong, P. Draper, A. El-Khadra, N. Gemelke, M. Hanada, D. Kharzeev, H. Lamm, Y.-Y. Li, J. Liu, M. Lukin, Y. Meurice, C. Monroe, B. Nachman, G. Pagano, J. Preskill, E. Rinaldi, A. Roggero, D. I. Santiago, M. J. Savage, I. Siddiqi, G. Siopsis, D. Van Zanten, N. Wiebe, Y. Yamauchi, K. Yeter-Aydeniz, and S. Zorzetti, Quantum simulation for high-energy physics, *PRX Quantum* **4**, 027001 (2023).
 [7] M. Kormos, M. Collura, G. Takács, and P. Calabrese, Real-time confinement following a quantum quench to a non-integrable model, *Nature Physics* **13**, 246–249 (2016).
 [8] Z.-Y. Ge and F. Nori, Confinement-induced enhancement of superconductivity in a spin- $\frac{1}{2}$ fermion chain coupled to a F_2 lattice gauge field, *Phys. Rev. B* **107**, 125141 (2023).
 [9] Z.-Y. Ge, Y.-R. Zhang, and F. Nori, Nonmesonic quantum many-body scars in a 1d lattice gauge theory, *Phys. Rev. Lett.* **132**, 230403 (2024).
 [10] E. A. Martinez, C. A. Muschik, P. Schindler, D. Nigg, A. Erhard, M. Heyl, P. Hauke, M. Dalmonte, T. Monz, P. Zoller, and R. Blatt, Real-time dynamics of lattice gauge theories with a few-qubit quantum computer, *Nature* **534**, 516–519 (2016).
 [11] H. Bernien, S. Schwartz, A. Keesling, H. Levine, A. Omran, H. Pichler, S. Choi, A. S. Zibrov, M. Endres, M. Greiner, V. Vuletić, and M. D. Lukin, Probing many-body dynamics on a 51-atom quantum simulator, *Nature* **551**, 579–584 (2017).
 [12] D. Gonzalez-Cuadra, M. Hamdan, T. V. Zache, B. Braverman, M. Kornjaca, A. Lukin, S. H. Cantu, F. Liu, S.-T. Wang, A. Keesling, M. D. Lukin, P. Zoller, and A. Bylinskii, Observation of string breaking on a $(2 + 1)$ d rydberg quantum simulator, *arXiv preprint arXiv:2410.16558* (2024).
 [13] Y. Liu, W.-Y. Zhang, Z.-H. Zhu, M.-G. He, Z.-S. Yuan, and J.-W. Pan, String breaking mechanism in a lattice schwinger model simulator, *arXiv preprint arXiv:2411.15443* (2024).
 [14] A. De, A. Lerose, D. Luo, F. M. Surace, A. Schuckert, E. R. Bennowitz, B. Ware, W. Morong, K. S. Collins, Z. Davoudi, *et al.*, Observation of string-breaking dynamics in a quantum simulator, *arXiv preprint arXiv:2410.13815* (2024).
 [15] T. A. Cochran, B. Jobst, E. Rosenberg, Y. D. Lensky, G. Gyawali, N. Eassa, M. Will, D. Abanin, R. Acharya, L. A. Beni, *et al.*, Visualizing dynamics of charges and strings in $(2+ 1)$ d lattice gauge theories, *arXiv preprint arXiv:2409.17142* (2024).
 [16] X. Liang, Z. Yue, Y.-X. Chao, Z.-X. Hua, Y. Lin, M. K. Tey, and L. You, *Observation of anomalous in-*

- formation scrambling in a rydberg atom array (2024), [arXiv:2410.16174 \[quant-ph\]](#).
- [17] R. C. Farrell, M. Illa, A. N. Ciavarella, and M. J. Savage, Quantum simulations of hadron dynamics in the schwinger model using 112 qubits, *Phys. Rev. D* **109**, 114510 (2024).
- [18] G. Lagnese, F. M. Surace, M. Kormos, and P. Calabrese, False vacuum decay in quantum spin chains, *Phys. Rev. B* **104**, L201106 (2021).
- [19] Z.-H. Zhu, Y. Liu, G. Lagnese, F. M. Surace, W.-Y. Zhang, M.-G. He, J. C. Halimeh, M. Dalmonte, S. C. Morampudi, F. Wilczek, *et al.*, Probing false vacuum decay on a cold-atom gauge-theory quantum simulator, [arXiv preprint arXiv:2411.12565 \(2024\)](#).
- [20] H. Ritsch, P. Domokos, F. Brennecke, and T. Esslinger, Cold atoms in cavity-generated dynamical optical potentials, *Rev. Mod. Phys.* **85**, 553 (2013).
- [21] F. Mivehvar, F. Piazza, T. Donner, and H. Ritsch, Cavity qed with quantum gases: new paradigms in many-body physics, *Advances in Physics* **70**, 1–153 (2021).
- [22] F. Schlawin, D. M. Kennes, and M. A. Sentef, Cavity quantum materials, *Applied Physics Reviews* **9**, 011312 (2022).
- [23] J. Bloch, A. Cavalleri, V. Galitski, M. Hafezi, and A. Rubio, Strongly correlated electron–photon systems, *Nature* **606**, 41 (2022).
- [24] F. J. Garcia-Vidal, C. Ciuti, and T. W. Ebbesen, Manipulating matter by strong coupling to vacuum fields, *Science* **373**, eabd0336 (2021).
- [25] J. Léonard, A. Morales, P. Zupancic, T. Esslinger, and T. Donner, Supersolid formation in a quantum gas breaking a continuous translational symmetry, *Nature* **543**, 87–90 (2017).
- [26] W. Nie, M. Antezza, Y.-x. Liu, and F. Nori, Dissipative topological phase transition with strong system-environment coupling, *Phys. Rev. Lett.* **127**, 250402 (2021).
- [27] T. Chanda, R. Kraus, G. Morigi, and J. Zakrzewski, Self-organized topological insulator due to cavity-mediated correlated tunneling, *Quantum* **5**, 501 (2021).
- [28] G. Chiriaco, M. Dalmonte, and T. Chanda, Critical light-matter entanglement at cavity mediated phase transitions, *Phys. Rev. B* **106**, 155113 (2022).
- [29] R. J. Valencia-Tortora, S. P. Kelly, T. Donner, G. Morigi, R. Fazio, and J. Marino, Crafting the dynamical structure of synchronization by harnessing bosonic multilevel cavity qed, *Phys. Rev. Res.* **5**, 023112 (2023).
- [30] G.-L. Zhu, C.-S. Hu, H. Wang, W. Qin, X.-Y. Lü, and F. Nori, Nonreciprocal superradiant phase transitions and multicriticality in a cavity qed system, *Phys. Rev. Lett.* **132**, 193602 (2024).
- [31] M. Schiró, M. Bordyuh, B. Öztöp, and H. E. Türeci, Phase transition of light in cavity qed lattices, *Phys. Rev. Lett.* **109**, 053601 (2012).
- [32] O. Viehmann, J. von Delft, and F. Marquardt, Observing the nonequilibrium dynamics of the quantum transverse-field ising chain in circuit qed, *Phys. Rev. Lett.* **110**, 030601 (2013).
- [33] M. Dalmonte, S. I. Mirzaei, P. R. Muppalla, D. Marcos, P. Zoller, and G. Kirchmair, Realizing dipolar spin models with arrays of superconducting qubits, *Phys. Rev. B* **92**, 174507 (2015).
- [34] J. Gelhausen, M. Buchhold, A. Rosch, and P. Strack, Quantum-optical magnets with competing short- and long-range interactions: Rydberg-dressed spin lattice in an optical cavity, *SciPost Phys.* **1**, 004 (2016).
- [35] Z. Li, S. Choudhury, and W. V. Liu, Fast scrambling without appealing to holographic duality, *Phys. Rev. Res.* **2**, 043399 (2020).
- [36] Z. Li, S. Choudhury, and W. V. Liu, Long-range-ordered phase in a quantum heisenberg chain with interactions beyond nearest neighbors, *Phys. Rev. A* **104**, 013303 (2021).
- [37] T. O. Puel and T. Macrì, Confined meson excitations in rydberg-atom arrays coupled to a cavity field, *Phys. Rev. Lett.* **133**, 106901 (2024).
- [38] A. Chiochetta, D. Kiese, C. P. Zelle, F. Piazza, and S. Diehl, Cavity-induced quantum spin liquids, *Nature Communications* **12**, 5901 (2021).
- [39] F. Mattiotti, J. Dubail, D. Hagenmüller, J. Schachenmayer, J.-P. Brantut, and G. Pupillo, Multifractality in the interacting disordered tavis-cummings model, *Phys. Rev. B* **109**, 064202 (2024).
- [40] A. Mallick, M. Lewenstein, J. Zakrzewski, and M. Płodzień, String breaking dynamics in ising chain with local vibrations (2024), [arXiv:2501.00604](#).
- [41] G. Jarc, S. Y. Mathengattil, A. Montanaro, F. Giusti, E. M. Rigoni, R. Sergo, F. Fassioi, S. Winnerl, S. Dal Zilio, D. Mihailovic, P. Prelovšek, M. Eckstein, and D. Fausti, Cavity-mediated thermal control of metal-to-insulator transition in 1T-TaS₂, *Nature* **622**, 487 (2023).
- [42] F. Appugliese, J. Enkner, G. L. Paravicini-Bagliani, M. Beck, C. Reichl, W. Wegscheider, G. Scalari, C. Ciuti, and J. Faist, Breakdown of topological protection by cavity vacuum fields in the integer quantum Hall effect, *Science* **375**, 1030 (2022).
- [43] J. Enkner, L. Graziotto, F. Appugliese, V. Rokaj, J. Wang, M. Ruggenthaler, C. Reichl, W. Wegscheider, A. Rubio, and J. Faist, Testing the renormalization of the von klitzing constant by cavity vacuum fields, *Phys. Rev. X* **14**, 021038 (2024).
- [44] J. Enkner, L. Graziotto, D. Boriçi, F. Appugliese, C. Reichl, G. Scalari, N. Regnault, W. Wegscheider, C. Ciuti, and J. Faist, Enhanced fractional quantum hall gaps in a two-dimensional electron gas coupled to a hovering splitting resonator (2024), [arXiv:2405.18362 \[cond-mat.mes-hall\]](#).
- [45] Z. Bacciconi, H. Xavier, I. Carusotto, T. Chanda, and M. Dalmonte, Theory of fractional quantum hall liquids coupled to quantum light and emergent graviton-polaritons (2024), [arXiv:2405.12292 \[cond-mat.mes-hall\]](#).
- [46] D.-P. Nguyen, G. Arwas, Z. Lin, W. Yao, and C. Ciuti, Electron-photon chern number in cavity-embedded 2d moiré materials, *Phys. Rev. Lett.* **131**, 176602 (2023).
- [47] D. Hagenmüller, J. Schachenmayer, S. Schütz, C. Genes, and G. Pupillo, Cavity-enhanced transport of charge, *Phys. Rev. Lett.* **119**, 223601 (2017).
- [48] Z. Bacciconi, G. M. Andolina, and C. Mora, Topological protection of Majorana polaritons in a cavity, *Phys. Rev. B* **109**, 165434 (2024).
- [49] Z. Yan, J. Ho, Y.-H. Lu, S. J. Masson, A. Asenjo-Garcia, and D. M. Stamper-Kurn, Super-radiant and sub-radiant cavity scattering by atom arrays (2023), [arXiv:2307.13321 \[quant-ph\]](#).
- [50] J. Ho, Y.-H. Lu, T. Xiang, C. C. Rusconi, S. J. Masson, A. Asenjo-Garcia, Z. Yan, and D. M. Stamper-Kurn, *Op-*

- tomemchanical self-organization in a mesoscopic atom array (2024), [arXiv:2410.12754](https://arxiv.org/abs/2410.12754) [quant-ph].
- [51] A. Browaeys and T. Lahaye, Many-body physics with individually controlled rydberg atoms, *Nature Physics* **16**, 132–142 (2020).
- [52] D. Bluvstein, S. J. Evered, A. A. Geim, S. H. Li, H. Zhou, T. Manovitz, S. Ebadi, M. Cain, M. Kalinowski, D. Hangleiter, J. P. Bonilla Ataides, N. Maskara, I. Cong, X. Gao, P. Sales Rodriguez, T. Karolyshyn, G. Semeghini, M. J. Gullans, M. Greiner, V. Vuletić, and M. D. Lukin, Logical quantum processor based on reconfigurable atom arrays, *Nature* **626**, 58–65 (2023).
- [53] S. R. White, Density matrix formulation for quantum renormalization groups, *Phys. Rev. Lett.* **69**, 2863 (1992).
- [54] U. Schollwöck, The density-matrix renormalization group in the age of matrix product states, *Annals of Physics* **326**, 96–192 (2011).
- [55] M. Yang and S. R. White, Time-dependent variational principle with ancillary Krylov subspace, *Phys. Rev. B* **102**, 094315 (2020).
- [56] C.-M. Halati, A. Sheikhan, H. Ritsch, and C. Kollath, Numerically exact treatment of many-body self-organization in a cavity, *Phys. Rev. Lett.* **125**, 093604 (2020).
- [57] Z. Bacciconi, G. M. Andolina, T. Chanda, G. Chiriacò, M. Schirò, and M. Dalmonte, First-order photon condensation in magnetic cavities: A two-leg ladder model, *SciPost Phys.* **15**, 113 (2023).
- [58] See Supplementary Material at [URL will be inserted by publisher] for further details on the model derivation, experimental remarks, state preparation and ground state properties..
- [59] Z.-Y. Ge, H. Fan, and F. Nori, Effective field theories and finite-temperature properties of zero-dimensional super-radiant quantum phase transitions, *Phys. Rev. Res.* **6**, 023123 (2024).
- [60] F. Minganti, I. I. Arkhipov, A. Miranowicz, and F. Nori, Continuous dissipative phase transitions with or without symmetry breaking, *New Journal of Physics* **23**, 122001 (2021).
- [61] F. Minganti, I. I. Arkhipov, A. Miranowicz, and F. Nori, Liouvillian spectral collapse in the scully-lamb laser model, *Phys. Rev. Res.* **3**, 043197 (2021).
- [62] J. Rohn, M. Hörmann, C. Genes, and K. P. Schmidt, Ising model in a light-induced quantized transverse field, *Phys. Rev. Res.* **2**, 023131 (2020).
- [63] Note that the classical meson density is a good indication of the presence of a meson only when this is close to its classical configuration, i.e. when $\delta \gg g$.
- [64] M. Saffman, Quantum computing with atomic qubits and rydberg interactions: progress and challenges, *Journal of Physics B: Atomic, Molecular and Optical Physics* **49**, 202001 (2016).
- [65] S. Ma, A. P. Burgers, G. Liu, J. Wilson, B. Zhang, and J. D. Thompson, Universal gate operations on nuclear spin qubits in an optical tweezer array of ^{171}Yb atoms, *Phys. Rev. X* **12**, 021028 (2022).
- [66] T. Thiele, J. Deiglmayr, M. Stammeier, J.-A. Agner, H. Schmutz, F. Merkt, and A. Wallraff, Imaging electric fields in the vicinity of cryogenic surfaces using rydberg atoms, *Phys. Rev. A* **92**, 063425 (2015).
- [67] Y.-T. Chen, M. Szurek, B. Hu, J. de Hond, B. Braverman, and V. Vuletic, High finesse bow-tie cavity for strong atom-photon coupling in rydberg arrays, *Optics Express* **30**, 37426 (2022).
- [68] R. C. Das, S. Khan, T. Ravi, and K. Pandey, Direct spectroscopy of rubidium using a narrow-line transition at 420 nm, *The European Physical Journal D* **78**, 10.1140/epjd/s10053-024-00831-9 (2024).
- [69] M. Fishman, S. R. White, and E. M. Stoudenmire, The ITensor Software Library for Tensor Network Calculations, *SciPost Phys. Codebases* , 4 (2022).
- [70] <https://github.com/titaschanda/TenNetLib.jl>.
- [71] J. Johansson, P. Nation, and F. Nori, Qutip: An open-source python framework for the dynamics of open quantum systems, *Computer Physics Communications* **183**, 1760–1772 (2012).